Ultrasonic preparation, stability and thermal conductivity of a capped copper - methanol nanofluid

Graves, J., Latvyte, E., Greenwood, A. & Emekwuru, N.

Original citation & hyperlink:
Graves, J, Latvyte, E, Greenwood, A & Emekwuru, N 2019, 'Ultrasonic preparation, stability and thermal conductivity of a capped copper - methanol nanofluid' Ultrasonics Sonochemistry, vol. (In-press), pp. (In-press).
https://dx.doi.org/10.1016/j.ultsonch.2019.02.028

DOI 10.1016/j.ultsonch.2019.02.028
ISSN 1350-4177
ESSN 1873-2828

Publisher: Elsevier

Ultrasonic preparation, stability and thermal conductivity of a capped copper - methanol nanofluid

J.E. Graves[a], E. Latvytė[b], A. Greenwood[b], N. G. Emekwuru[a,c]

[a] *Research Institute for Future Transport and Cities, Coventry University, Coventry, CV1 2DS, United Kingdom*

[b] *Faculty of Health and Life Sciences, Coventry University, CV1 2DS, United Kingdom.*

[c]*Faculty of Engineering, Environment and Computing, Coventry University, Coventry, CV1 2JH, United Kingdom.*

Abstract

This paper describes a two-step method to prepare novel copper-methanol nanofluids capped with a short chain molecule, (3-Aminopropyl)trimethoxysilane (APTMS). Two commercial nanopowders were dispersed at various powers using a 20 kHz ultrasonic probe into solutions of methanol and the capping agent. Ultrasonic energy input was measured by calorimetry with z-average diameters, intensity and number size distributions recorded by a dynamic light scattering technique. The stability of the dispersion was monitored visually, and quantified by recording the zeta potential. Dispersions of the bare powder were used as a control. Absorption spectroscopy was used to confirm the presence of the capping agent. The thermal conductivities of 0 to 10 % wt./vol. (1.1 % vol.) dispersions of the capped copper-methanol nanofluid were determined using a C-Therm analyzer. Optimum ultrasonic de-agglomeration conditions gave dispersions with a z-average particle size of < 200 nm and a PdI of < 0.2. The capped particles showed good stability; up to six months in some instances, and an average zeta potential of + 38 mV was recorded. The thermal conductivity of the nanofluid increased with concentration, and an enhancement of 9% over the base

fluid was found at 10 % wt./vol. (1.1% vol.). This innovative work has demonstrated the ultrasonic preparation and stability of copper nanoparticles protected with APTMS; a short chain molecule which binds to copper and prevents oxidation. The protected particles can enhance the thermal conductivity of methanol with no interference from the capping ligand.

Keywords: copper nanoparticles; methanol; nanofluids; nanorefrigerant; particle size; thermal conductivity; thermofluids; ultrasonic dispersion; zeta potential.

1. Introduction

Many engineering applications, such as refrigeration, direct solar collectors [1], automobile radiators [2] and the cooling of central processing units in electronic systems [3] use heat exchangers to transfer heat between two or more fluids. Heat exchangers are a critical component of any system and should work efficiently. Although various methods have been used to improve their performance, success is often limited by the thermal conductivity of the transfer fluid.

One possible method of enhancing thermal conductivity of fluids is to add particles with a high thermal conductivity to form a dispersion of the solid in the base fluid. However when particle sizes are of the order of millimetres or micrometres, the suspensions are unstable, and the solids simply separate out and become ineffective. Because of their small size, nanoparticles offer a greater chance of producing stable dispersions. Since Choi et al. [4] conceived the concept of nanofluids, many researchers are working actively on nanofluid systems for heat transfer applications [5–8].

Nanoparticle metal oxides are routinely added as additives to base fluids due to their relatively high thermal conductivity, low cost, and compatibility [9]. Typically, aluminium, copper, silicon, titanium, and zinc oxides have been studied and their

effect on thermal conductivity at different particle concentrations has been recorded [10–14] . Nanofluids containing base metals such as gold, silver and copper have also been prepared [15–17] . Copper is a relatively low cost base metal, with a very high thermal conductivity (401 W / m K), second only to silver, and is approximately one order of magnitude higher than copper oxide. Reported enhanced thermal conductivity values for copper range from 2 to 78% [8]. However, when metallic nanoparticles are introduced to a base fluid they often have poor stability. Stability is a critical issue for nanofluids [18,19] and is considered to be one of most challenging factors limiting their practical use and further development.

For metals such as copper, dispersion stability can be improved by applying long chain surface capping ligands [20–22] or by the addition of polymer dispersants [23,24]. This can be achieved through a one or two-step preparation method [25]. Ultrasonication is regarded as a critical part of the two step process [25] and ultimately influences the quality and stability of the prepared dispersion. Ghadimi et al. [26] reviewed ultrasonic experimental conditions and Haddad et al. [18] reviewed methods for the preparation of aqueous, oil and ethylene glycol copper nanofluids. They stated that in all the copper preparation methods reviewed the nanofluids were not stable for more than one month. Graves et al. [27,28] studied the ultrasonic dispersion and particle size of bare and functionalised APTMS copper nanopowders in propan-2-ol, for applications in electronics manufacturing. The capped powders showed good dispersion characteristics and remained stable for long periods after 30 min of ultrasonic dispersion with a z-average of 165 nm and a polydispersity value of 0.17.

This work investigates the use of methanol as a base fluid for capped copper nanopowders. Methanol has useful properties; it can provide good protection against

freezing and can be used in solar adsorption refrigeration systems. Previous work has reported on the thermal conductivities of methanol / oxide systems [10,11,29] for various applications [30,31], and also reported enhanced thermal conductivities ranging from 10 to 30%. Capped copper nanopowder / methanol solutions have not been investigated. We report for the first time on the ultrasonic preparation; particle size; stability and thermal conductivity of APTMS capped copper nanoparticles in methanol. We have identified optimised ultrasonic processing conditions to produce a nanofluid which has demonstrated good stability and enhanced thermal conductivity.

2. Materials, Equipment and Methods

2.1. Materials

Copper nanopowders, unprotected, were purchased from two sources; SkySpring Nanomaterials Inc. (Product #:0800SJ, 25 nm Ø, 99.8% Cu, supplier 1) and Sigma-Aldrich (Product Code: 774081-5G, 25 nm Ø by TEM, supplier 2). Commercial powders were used to eliminate issues with product variation and to consider the potential for large scale use of the materials in any 'end' application. They were supplied in the form of dry powders contained in either sealed pouches or airtight glass containers. The copper particles were stored and dispensed in a nitrogen filled glove box. Methanol (high performance liquid chromatography grade, HPLC) was purchased from Fisher-Scientific and was used as supplied. The capping agent, (3-Aminopropyl)trimethoxysilane (APTMS), was supplied as a 97% liquid by Sigma-Aldrich. Further material properties are listed in Table 1.

2.2. Equipment

Micrographs of the powders were recorded using a Carl Zeiss 1530 VP field emission gun scanning electron microscope (FEGSEM). To prepare the samples, copper powder was brushed onto adhesive carbon supports placed on aluminium stubs. A 20 kHz Sonic and Materials Inc. VC 750 Ultrasonic Processor with a maximum electrical energy output of 750 W was used for dispersing the powders into methanol. The unit was fitted with a solid 1.3 cm diameter horn. The ultrasonic probe was calibrated with methanol using the calorimetry method [32]. HPLC grade methanol (100 cm^3) was sonicated for 5 minutes and the temperature increase was recorded using a thermocouple-type thermometer. The experiment was repeated three times for each amplitude. Energy densities of 0.07, 0.18, 0.32 and 0.42 W cm^{-3} were

calculated at 20, 40, 60 and 80 % amplitudes respectively. Power intensities of 5, 14, 24 and 32 W cm^{-2} were calculated for these amplitudes.

The particle size of the dispersed nanofluid was measured using a Dynamic Light Scattering (DLS) instrument (Malvern Zetasizer NanoS). Z-average diameters (mean cluster size based on the intensity of scattered light), intensity and number based size distributions were recorded. Each measurement consisted of 12 runs and there were three measurements automatically taken for each sample. A material absorption value of 1.00 was used for copper. Zeta potential measurements were measured by Electrophoretic Light Scattering (ELS) using a Malvern Zetasizer Nano ZSP. Preparation solutions were visually inspected every 24 hours and photographs taken to monitor stability. A Shimadzu UV-1800 UV/VIS spectrophotometer was used to confirm the presence of nanoparticles.

The thermal conductivities of nanofluid dispersions were measured using a C-Therm TCi Thermal Conductivity analyser by applying a known current to the sensor's spiral heating element. The C-Therm MTPS method applied a low energy pulse for a very short time (0.8 s) so that the thermal conductivity measurement was not influenced by thermal convection. Three readings were taken for each dispersion and the average calculated. The readings were recorded at 22ºC. Methanol and a standard foam were used as control samples. The precision of the C-Therm is ~ 1 %, while the accuracy of the measurements is < 4 %.

2.3. Methods

A two-step preparation method (represented schematically in Figure 1.) was used to prepare bare and capped copper nanofluids using a similar procedure described in [27,28]. Typically, 0.1 g of copper nanopowder was added to 100 cm^3 of methanol in a 150 cm^3 tall glass beaker to produce a 0.1 % wt./vol. mixture. The

capped particles were prepared by adding APTMS (175 μL) to the methanol prior to the addition of the copper powder. A 20 kHz ultrasonic probe was used to disperse the particles. The capped nanoparticles were separated from any excess APTMS molecules by centrifugation. The supernatant was decanted; the remaining solid washed with methanol and the process repeated before a final ultrasonic treatment was applied. All samples were analysed by DLS and then transferred into glass vials for monitoring and thermal conductivity testing.

3. Results and Discussion

3.1 Copper nanoparticle morphology

SEMs of the 'as supplied' dry copper nanopowders are shown in Figure 2(a) and (b). The particles from both suppliers were of similar appearance; large irregular sphere shaped particles were observed, and sizeable clusters were present which were agglomerates of the primary particles. A primary particle size of 25 to 75 nm Ø was observed for the powder from supplier 1, Figure (a). The results are very similar to those reported in [27]. The SEM image of the powder sourced from supplier 2 showed primary particles between 25 to 250 nm Ø, Figure (b). Both images presented a structure which was liable to disruption under sonication. The powder samples were sputter coated. Hence the mottled effect observed on the surface of the particles.

3.2 Ultrasonic dispersion of bare and capped nanopowders

Ultrasonic dispersion using a 20 kHz horn is very effective at de-agglomerating copper nanopowders. Protecting the copper surface, which is prone to oxidation, with a short chain molecule such as APTMS can be an effective means of capping the clusters and stabilising the dispersion [28]. APTMS is soluble in methanol and can be added to the base fluid before the copper nanopowder and ultrasonic dispersion takes place. Nanopowder from supplier 1 was used to study the effect of ultrasonic amplitude on dispersion particle size for bare and capped APTMS particles. Figure 3(a) shows a plot of the z-average value as a function of amplitude after 30 minutes of ultrasonic processing for nanopowders in methanol, 0.1 % wt./vol. For the bare particles it was difficult to measure the particle size distribution with great confidence because of the interference from micron sized agglomerates, which scatter significantly more light than nanoparticles. In particular, large variations in the z-average size were observed at lower amplitudes; the result at 40% amplitude

demonstrates this type of interference. For powders dispersed in the presence of APTMS the results could be reproduced with consistency at low and high amplitudes. They also showed a gradual decrease in z-average with increasing ultrasonic amplitude from 330nm at 20% to 190 nm at 80%.

Typical intensity plots for the lowest and highest amplitudes applied to the capping solution are shown in Figure 3(b). After 30 minutes of processing at 20 % amplitude, two peaks were recorded at 340 nm and 4690 nm and the z-average and polydispersity index (PdI) were 330 nm and 0.229 respectively. At 80% amplitude, the peak was shifted to the left and a unimodal distribution was observed. The recorded z-average was 190 nm and the PdI was 0.162. The size distribution number plot, Figure 3 (c) also showed a shift in peak position to lower particle sizes as the amplitude was increased, with a maximum peak height at 105 nm. Clearly, higher ultrasonic operating amplitudes lead to greater agglomeration breakage rates, along with a reduction in the size of the capped copper nanopowder clusters, as reported in previous work with propan-2-ol [27,28]. Optimum de-agglomeration conditions were established at 80 % amplitude and 30 min processing time. Typically, this gave a significant proportion of 100 nm capped clusters and a z-average of 190 nm. A higher amplitude of 100% was tested, but the heat generated during the 30 min processing period caused significant loss of methanol base fluid.

To simplify the experimental design, a comparison of the dispersion characteristics of the two capped nanopowders was undertaken. Size distribution-intensity plots after 30 minutes of ultrasonic processing at 80% amplitude are shown in Figure 4. Again, fragmentation of the large agglomerates was observed and the size distribution was unimodal for both nanopowders. A slight shoulder at lower size diameters was recorded for supplier 2 which would suggest the presence of a second

population of smaller sized nanoparticles. As a consequence, lower z-average and higher polydispersity index values (167 nm and 0.210) were recorded in comparison with powder 1 (190 nm and 0.162). The presence of the smaller sized particles has decreased the z-average value but has increased the size range of particles present in the dispersion. Based on this experiment the difference between the two commercial powders was deemed to be insignificant and therefore further experiments were performed only with the nanopowder from supplier 2.

3.3 Nanofluid stability

Bare and capped particles were prepared using optimum ultrasonic conditions and then set aside in glass vials in order to assess the short term stability of the prepared nanofluids. DLS measurements were taken both at preparation and after 24, 48 and 72 hours, to record the particle size. A plot of z-average versus time for the bare and capped dispersions is shown in Figure 5(a). Just after preparation, z-averages were similar to those which had been observed previously. With increasing time, the z-average decreased slightly and then maintained a steady value below 150 nm. Figure 5(b) and (c) record the intensity and number size distribution plots for the capped particles after 0 and 72 hours. The intensity peak has shifted to the left after 72 hours, indicating some sedimentation of larger particles. The number-size distribution plot also recorded a shift in peak population from a bimodal distribution to a unimodal distribution below 100nm.

However, it was obvious from photographs of the dispersions, Figure 6, that although both samples were fully dispersed after preparation (a,b); after 72 hours visible sedimentation had occurred in the glass vial containing bare particles (c) but not the capped particles (d). Figure 6(e) is a photograph of the bare particles taken after six months. It can be seen that complete sedimentation has taken place; the

copper particles have also changed appearance and colour (black to blue). For the capped particles, a small amount of sedimentation was observed, but a significant proportion of the powder remained dispersed (d) and in some cases samples retained their stability after six months of storage (f). A DLS measurement taken from sample (f) had a recorded z-average of 227 nm and a PdI of 0.237, higher values than after preparation but values which demonstrate long term stability.

In summary, for bare and uncapped particle types, during the first 24 hours after preparation, sedimentation of large nanoclusters occurs. The z-average then stabilises and remains constant. However, it can be seen from the photographs that the degree of sedimentation is significantly less for the capped particles. The APTMS molecule is very effective in binding to the copper, and even though it has a short chain length, it protects the copper from agglomerating and oxidising.

3.4 Absorption spectroscopy

To confirm the formation of a capped layer of APTMS molecules, further evidence was obtained by recording the absorption spectra from dispersed samples. Figure 7 shows spectra from (a) dispersed bare copper nanopowder (b) APTMS capped copper nanopowder (c) after the addition of glacial acetic acid (3.7 % by vol.) to the bare powder and (d-g) after the addition of glacial acetic acid to the capped particles. The absorption spectrum for the bare particles (a) showed a broad surface plasmon peak in the wavelength range 630 to 660 nm. The broadness of the peak was attributed to the presence of copper oxide [33] or the larger size / distribution of nanoparticles [34]. On addition of glacial acetic acid (which dissolves copper and copper oxides) to the dispersion of the bare particles; the surface plasmon peak disappeared completely in less than 1 min (c). The absorption spectrum for the capped particles was sharper and showed a blue shift in λ_{max} to 599 nm (b). On

addition of glacial acetic acid to the dispersion, the surface plasmon peak decreased slowly and red shifted before it disappeared after 8 minutes in the presence of the acid (d-g). Clearly, the APTMS molecule must be attached to the copper nanopowder and is providing a physical barrier to the acid through the formation of a densely packed layer of short chain molecules thereby, slowing down the dissolution of the core copper cluster.

APTMS is known to stabilise other metal nanoparticles such as silver [35] where it forms a complex through its amine functionality with the silane groups pointing towards the solution. For copper, it is unclear whether the group that attaches is the amine or the silane group, but in all probability the attachment is via the amine group. In previously unpublished angle resolved XPS results which investigated the attachment of APTMS films to copper foil, the silicon signal consistently appeared at the top of the sample and above the N 1s peak on the relative depth plot. So, however the molecule is attached, a favourable increase of particle stability and oxidation protection is observed [28] via the formation of a dense packed layer.

3.5 Zeta Potential Measurements

The zeta potential of the bare and capped particles was determined, see Figure 8. A positive zeta potential was recorded for both dispersions. The bare dispersions had an average zeta potential value of +23 mV in methanol. During repeat measurements, there appeared to be large fluctuations in the derived count rate which suggested the sample was sedimenting or changing over time. The APTMS capped sample had good repeatability between measurements, and exhibited a higher average zeta potential of +38 mV. For a physically-stable nanoparticle suspension to be stabilized solely by electrostatic repulsion, a zeta potential of ±30 mV (minimum) is required [36]. This suggests that we can regard the capped copper nanopowders as relatively

stable systems, with a reduced tendency for aggregation; whereas the bare particles show an increased tendency for agglomeration. Dispersion stability could also be brought about by the APTMS molecules overlapping and sterically stabilising the copper clusters.

3.6 Thermal conductivity measurements

The thermal conductivities of different concentrations of protected copper nanopowder / methanol dispersions were measured. Figure 9 shows the thermal conductivity of the dispersions as a function of concentration. Negligible enhancements were observed up to 2 % wt./vol., above which the thermal conductivity increased with nanopowder concentration, and the enhancement was observed to be 3.8 % and 9 % over the base fluid at the concentrations of 4 and 10 % wt./vol. (or 0.45 and 1.10 % vol.) respectively. These values are in agreement with previous studies which have used Cu NPs dispersed in ethylene glycol, diethylene glycol [37] and hydrocarbons [24] as the base fluid. However, they are significantly lower than those reported by other groups that have used Cu NP water based systems [23]. Researchers have also reported enhancement factors for methanol based fluids with nanoparticles other than copper; typically aluminium oxide and silicon dioxide where the enhancement factors have also been similar [10] or slightly higher [11] at lower % vol. Also, it is known that long chain molecules such as surfactants can affect the thermal conductivity of nanofluids [38, 39]. For APTMS-copper nanofluids, the evidence suggests that the short chain molecule does not interfere with the thermal conductivity; the data obtained is comparable with results reported in the literature for unprotected particles [37].

4. Conclusions

This work has demonstrated that an APTMS capped copper-methanol nanofluid can be prepared from commercial copper nanopowders using a 20 kHz ultrasonic probe. With carefully controlled ultrasonic processing conditions, 80% amplitude for 30 min at 32 W cm^{-2}; z-averages below 200 nm and a PdI < 0.2 can be achieved. The nanofluid has improved dispersion stability and resistance to oxidation when compared with bare copper nanopowders . An average zeta potential measurement of +38 mV was recorded for the capped particles in methanol and good stability for up to six months was observed in some instances. The thermal conductivity of the nanofluid dispersions was found to increase with concentration. A maximum enhancement of 9 % over pure methanol was observed at the highest concentration of 10 % wt./vol. (1.10 % vol.). This increase in thermal conductivity is comparable with oxide-methanol nanofluids of similar particle size. Many workers have acknowledged that particle size and shape are important factors and play a significant role in dynamic heat transfer reactions. In our set of experiments, we have monitored closely the particle size of the capped dispersions. Clearly, they are not monodisperse systems and ultrasound will not produce a uniform particle size, but the application of optimised ultrasonic parameters has de-agglomerated and narrowed the size distribution of the powders. This has allowed us to control important parameters which influence the thermal conductivity of the nanofluid.

Acknowledgements

The authors would like to thank Malvern Panalytical for measuring the zeta potential of the bare and capped dispersions. The study was supported by the Coventry University Undergraduate Research Experience Scheme (CUURES), the EU H2020

SARTEA – 661515 project, the Coventry University Faculty of Health and Life Sciences project fund, and the Research Institute for Future Transport and Cities project fund.

References

[1] V. Khullar, H. Tyagi, N. Hordy, T.P. Otanicar, Y. Hewakuruppu, P. Modi, R.A. Taylor, Harvesting solar thermal energy through nanofluid-based volumetric absorption systems, Int. J. Heat Mass Transf. 77 (2014) 377–384. doi:10.1016/j.ijheatmasstransfer.2014.05.023.

[2] S.S. Chougule, S.K. Sahu, Comparative Study of Cooling Performance of Automobile Radiator Using Al 2 O 3 -Water and Carbon Nanotube-Water Nanofluid, J. Nanotechnol. Eng. Med. (2014). doi:10.1115/1.4026971.

[3] A. Sakanova, S. Yin, J. Zhao, J.M. Wu, K.C. Leong, Optimization and comparison of double-layer and double-side micro-channel heat sinks with nanofluid for power electronics cooling, Appl. Therm. Eng. (2014). doi:10.1016/j.applthermaleng.2014.01.005.

[4] X. Wang, X. Xu, S.U. S. Choi, Thermal Conductivity of Nanoparticle - Fluid Mixture, J. Thermophys. Heat Transf. 13 (1999) 474–480. doi:10.2514/2.6486.

[5] C. Pang, J.W. Lee, Y.T. Kang, Review on combined heat and mass transfer characteristics in nanofluids, Int. J. Therm. Sci. 87 (2015) 49–67. doi:10.1016/j.ijthermalsci.2014.07.017.

[6] P.K. Das, A review based on the effect and mechanism of thermal conductivity of normal nanofluids and hybrid nanofluids, J. Mol. Liq. 240 (2017) 420–446. doi:10.1016/j.molliq.2017.05.071.

[7] R. Saidur, S.N. Kazi, M.S. Hossain, M.M. Rahman, H.A. Mohammed, A review on the performance of nanoparticles suspended with refrigerants and lubricating oils in refrigeration systems, Renew. Sustain. Energy Rev. 15 (2011) 310–323. doi:10.1016/j.rser.2010.08.018.

[8] S.A. Angayarkanni, J. Philip, Review on thermal properties of nanofluids: Recent developments, Adv. Colloid Interface Sci. 225 (2015) 146–176. doi:10.1016/j.cis.2015.08.014.

[9] D.K. Devendiran, V.A. Amirtham, A review on preparation, characterization, properties and applications of nanofluids, Renew. Sustain. Energy Rev. 60 (2016) 21–40. doi:10.1016/j.rser.2016.01.055.

[10] C. Pang, J.Y. Jung, J.W. Lee, Y.T. Kang, Thermal conductivity measurement of methanol-based nanofluids with Al2O3and SiO2nanoparticles, Int. J. Heat Mass Transf. 55 (2012) 5597–5602. doi:10.1016/j.ijheatmasstransfer.2012.05.048.

[11] R.M. Mostafizur, R. Saidur, A.R. Abdul Aziz, M.H.U. Bhuiyan, Thermophysical properties of methanol based Al2O3nanofluids, Int. J. Heat Mass Transf. 85 (2015) 414–419. doi:10.1016/j.ijheatmasstransfer.2015.01.075.

[12] Y. Guo, T. Zhang, D. Zhang, Q. Wang, Experimental investigation of thermal and electrical conductivity of silicon oxide nanofluids in ethylene glycol/water mixture, Int. J. Heat Mass Transf. 117 (2018) 280–286. doi:10.1016/j.ijheatmasstransfer.2017.09.091.

[13] P.B. Maheshwary, C.C. Handa, K.R. Nemade, A comprehensive study of effect of concentration, particle size and particle shape on thermal conductivity of titania/water based nanofluid, Appl. Therm. Eng. 119 (2017) 79–88. doi:10.1016/j.applthermaleng.2017.03.054.

[14] A. Ghadimi, I.H. Metselaar, The influence of surfactant and ultrasonic processing on improvement of stability, thermal conductivity and viscosity of titania nanofluid, Exp. Therm. Fluid Sci. 51 (2013) 1–9.

doi:10.1016/j.expthermflusci.2013.06.001.
[15] H.E. Patel, S.K. Das, T. Sundararajan, A. Sreekumaran Nair, B. George, T. Pradeep, Thermal conductivities of naked and monolayer protected metal nanoparticle based nanofluids: Manifestation of anomalous enhancement and chemical effects, Appl. Phys. Lett. (2003). doi:10.1063/1.1602578.
[16] M. Sato, Y. Abe, Y. Urita, R.D. Paola, A. Cecere, R. Savino, Thermal performance of self-rewetting fluid heat pipe containing dilute solutions of polymer capped silver nanoparticles synthesized by microwave-polyol process, Proceeding ITP 2009. 12 (2009) 339–345.
[17] S. Bhanushali, N.N. Jason, P. Ghosh, A. Ganesh, G.P. Simon, W. Cheng, Enhanced Thermal Conductivity of Copper Nanofluids: The Effect of Filler Geometry, ACS Appl. Mater. Interfaces. 9 (2017) 18925–18935. doi:10.1021/acsami.7b03339.
[18] Z. Haddad, C. Abid, H.F. Oztop, A. Mataoui, A review on how the researchers prepare their nanofluids, Int. J. Therm. Sci. 76 (2014) 168–189. doi:10.1016/j.ijthermalsci.2013.08.010.
[19] F. Yu, Y. Chen, X. Liang, J. Xu, C. Lee, Q. Liang, P. Tao, T. Deng, Dispersion stability of thermal nanofluids, Prog. Nat. Sci. Mater. Int. 27 (2017) 531–542. doi:10.1016/j.pnsc.2017.08.010.
[20] P.K. Khanna, T.S. Kale, M. Shaikh, N.K. Rao, C.V.V. Satyanarayana, Synthesis of oleic acid capped copper nano-particles via reduction of copper salt by SFS, Mater. Chem. Phys. 110 (2008) 21–25. doi:10.1016/j.matchemphys.2008.01.013.
[21] P. Kanninen, C. Johans, J. Merta, K. Kontturi, Influence of ligand structure on the stability and oxidation of copper nanoparticles, J. Colloid Interface Sci. 318 (2008) 88–95. doi:10.1016/j.jcis.2007.09.069.
[22] D.A. Hutt, C. Liu, Oxidation protection of copper surfaces using self-assembled monolayers of octadecanethiol, Appl. Surf. Sci. 252 (2005) 400–411. doi:10.1016/j.apsusc.2005.01.019.
[23] M. Saterlie, H. Sahin, B. Kavlicoglu, Y. Liu, O. Graeve, Particle size effects in the thermal conductivity enhancement of copper-based nanofluids, 6 (2011) 1–7. doi:10.1186/1556.
[24] D. Li, W. Xie, W. Fang, Preparation and properties of copper-oil-based nanofluids, (2011) 1–7.
[25] L. Kong, J. Sun, Y. Bao, Preparation, characterization and tribological mechanism of nanofluids, RSC Adv. 7 (2017) 12599–12609. doi:10.1039/c6ra28243a.
[26] A. Ghadimi, R. Saidur, H.S.C. Metselaar, A review of nanofluid stability properties and characterization in stationary conditions, Int. J. Heat Mass Transf. 54 (2011) 4051–4068. doi:10.1016/j.ijheatmasstransfer.2011.04.014.
[27] J.E. Graves, M. Sugden, R.E. Litchfield, D.A. Hutt, T.J. Mason, A.J. Cobley, Ultrasound assisted dispersal of a copper nanopowder for electroless copper activation, Ultrason. Sonochem. 29 (2016). doi:10.1016/j.ultsonch.2015.10.016.
[28] R.E. Litchfield, J. Graves, M. Sugden, D.A. Hutt, A. Cobley, Functionalised copper nanoparticles as catalysts for electroless plating, in: Proc. 16th Electron. Packag. Technol. Conf. EPTC 2014, 2014. doi:10.1109/EPTC.2014.7028381.
[29] R.M. Mostafizur, M.H.U. Bhuiyan, R. Saidur, A.R. Abdul Aziz, Thermal conductivity variation for methanol based nanofluids, Int. J. Heat Mass Transf. 76 (2014) 350–356. doi:10.1016/j.ijheatmasstransfer.2014.04.040.

[30] J.H. Kim, C.W. Jung, Y.T. Kang, Mass transfer enhancement during CO2 absorption process in methanol/Al2O3 nanofluids, Int. J. Heat Mass Transf. 76 (2014) 484–491. doi:10.1016/j.ijheatmasstransfer.2014.04.057.
[31] E. Firouzfar, M. Soltanieh, S.H. Noie, S.H. Saidi, Energy saving in HVAC systems using nanofluid, Appl. Therm. Eng. 31 (2011) 1543–1545. doi:10.1016/j.applthermaleng.2011.01.029.
[32] T.J. Mason, D. Peters, Practical Sonochemistry, 2nd ed., Ellis Horwood publishing, Chichester, 2002.
[33] George H. Chan, Jing Zhao, Erin M. Hicks, * and George C. Schatz, R.P. Van Duyne*, Plasmonic Properties of Copper Nanoparticles Fabricated by Nanosphere Lithography, (2007). doi:10.1021/NL070648A.
[34] I. Lisiecki, F. Billoudet, M.P. Pileni, Control of the Shape and the Size of Copper Metallic Particles, J. Phys. Chem. 100 (1996) 4160–4166. doi:10.1021/jp9523837.
[35] I. Pastoriza-Santos, L.M. Liz-Marzán, Binary cooperative complementary nanoscale interfacial materials. Reduction of silver nanoparticles in DMF. Formation of monolayers and stable colloids, Pure Appl. Chem. 72 (2000) 83–90. doi:10.1351/pac200072010083.
[36] R.J. Hunter, Zeta potential in colloid science : principles and applications, doi:10.1016/IC2013-0-07389-6.
[37] N. Nikkam, M. Ghanbarpour, R. Khodabandeh, M.S. Toprak, The effect of particle size and base liquid on thermo-physical properties of ethylene and diethylene glycol based copper micro- and nanofluids, Int. Commun. Heat Mass Transf. 86 (2017) 143–149. doi:10.1016/j.icheatmasstransfer.2017.05.026.
[38] G. Xia, H. Jiang, R. Liu, Y, Zhai, Effects of surfactant on the stability and thermal conductivity of Al_2O_3/de-ionized water nanofluids, Int. J of Thermal Sci. 84 (2014) 118-124. doi:10.1016/j.ijthermalsci.2014.05.004
[39] M.Z. Zhou, G.D. Xia, J. Li, L. Chai, L.J. Zhou, Analysis of factors influencing thermal conductivity and viscosity in different kinds of surfactant solutions, Exp. Therm. Fluid Sci. 36 (2012) 22- 29. doi: 10.1016/j.expthermflusci.2011.07.014

Table 1. Properties of the materials used.

Parameter	Cu	Methanol	APTMS
Molecular mass / (g/mol)	63.55	32.04	179.3
Density / (g/cm^3)	8.96	0.792	1.027
Thermal Conductivity / (W/m K)	401	0.204	-

Figure Legends

Figure 1. Schematic of the nanofluid preparation sequence.

Figure 2. Scanning electron micrographs of ‘as received’ nanoparticles (a) supplier 1 (b) supplier 2.

Figure 3. (a) A plot of the mean particle size versus ultrasonic amplitude (20 kHz, 30 min) for bare and capped copper nanoparticles and (b) intensity vs size distribution and (c) number vs size distribution plots for capped nanoparticles.

Figure 4. A plot of intensity vs size distribution of capped copper nanopowders prepared from supplier 1 and 2, bare copper nanopowder, ultrasonic processing conditions (80% amplitude, 20 kHz).

Figure 5. (a) A plot of the mean particle size versus time for bare and capped copper nanowders (b) intensity vs size distribution and (c) number vs size distribution plots for capped nanoparticles.

Figure 6. Photographs of bare and capped dispersions (a,b) after preparation (c,d) after 72 h (e,f) and after six months of storage.

Figure 7. Absorption spectra of dispersions of (a) bare (b) capped copper nanoparticles (c) bare plus glacial acetic acid, 1min (d-g) capped plus glacial acetic acid, 2,4,6,8 min.

Figure 8. Typical Zeta potential distribution for bare and capped copper nanoparticles in methanol, 0.1 % wt./vol. concentration.

Figure 9. Thermal conductivity of protected copper nanoparticle – methanol dispersions as a function of concentration, T= 22ºC.

Figure 1.

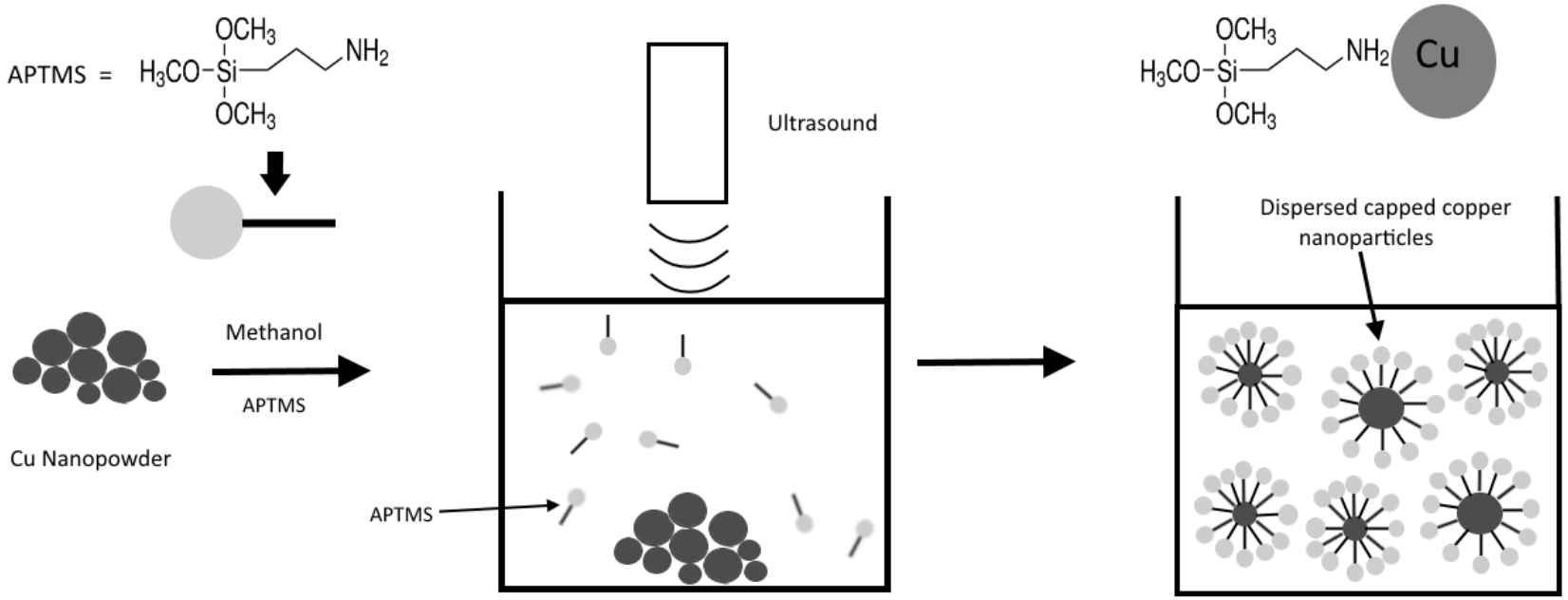
APTMS =
OCH3
H3CO–Si
NH2
OCH3
Ultrasound
Methanol
APTMS
Cu Nanopowder
APTMS
Cu
Dispersed capped copper nanoparticles

Figure 2.

(a)

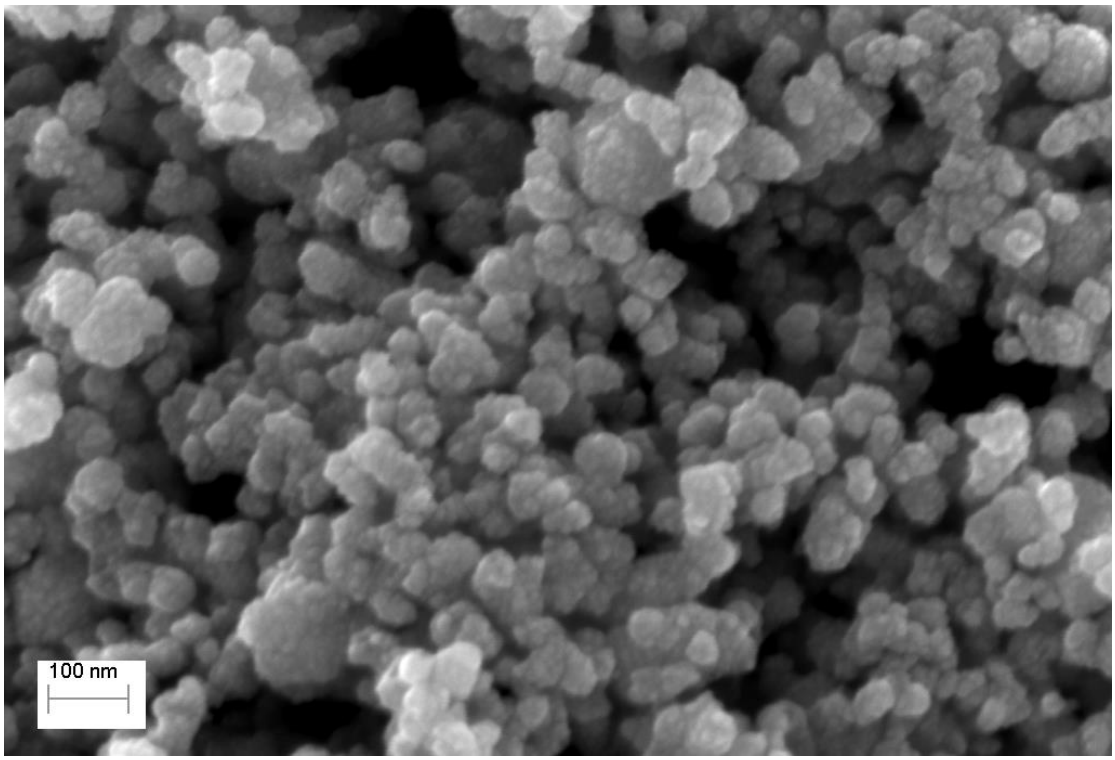

(b)

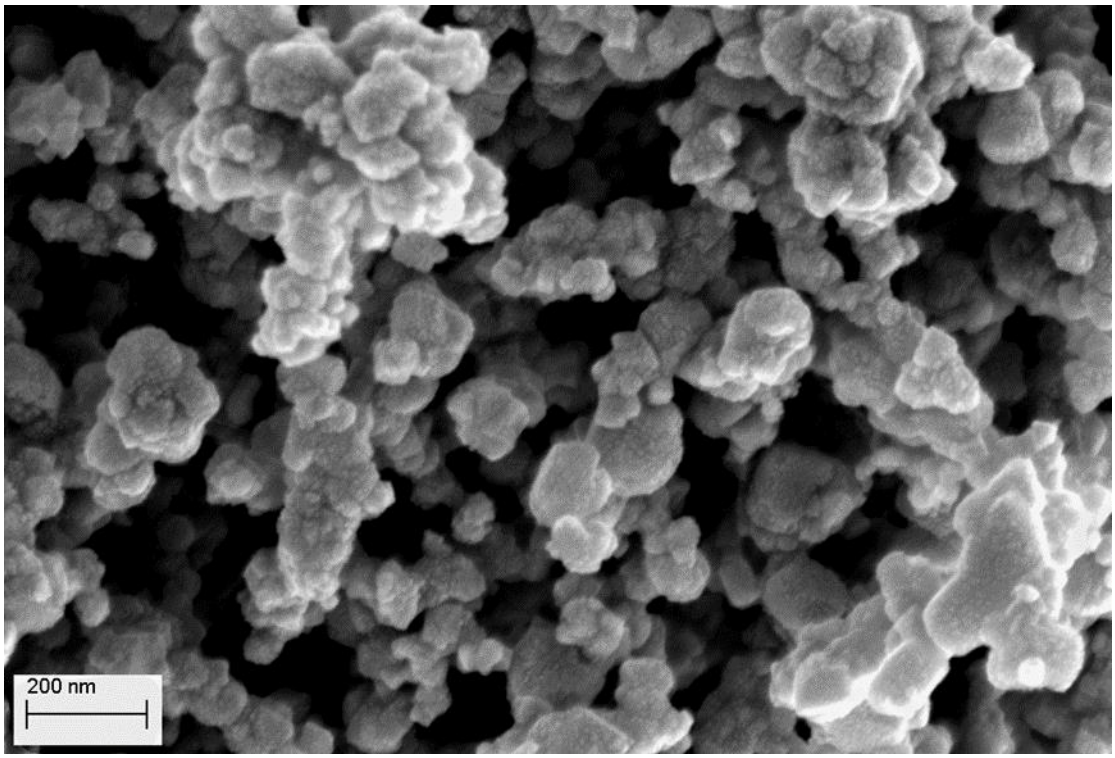

Figure 3.

(a)

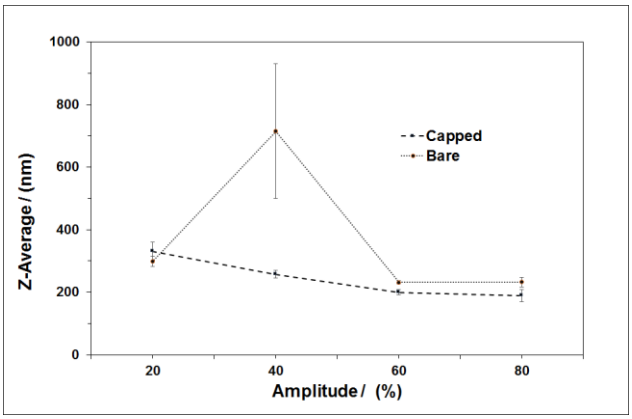
Z-Average / (nm)
Amplitude / (%)
Capped
Bare
0
200
400
600
800
1000
20
40
60
80

(b)

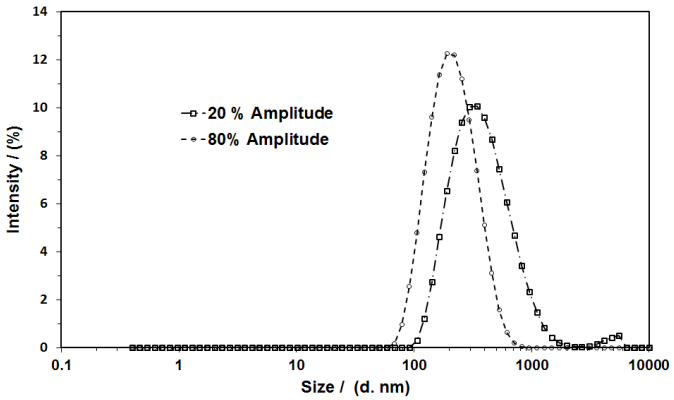
Intensity / (%)
Size / (d. nm)
20 % Amplitude
80% Amplitude
0
2
4
6
8
10
12
14
0.1
1
10
100
1000
10000

(c)

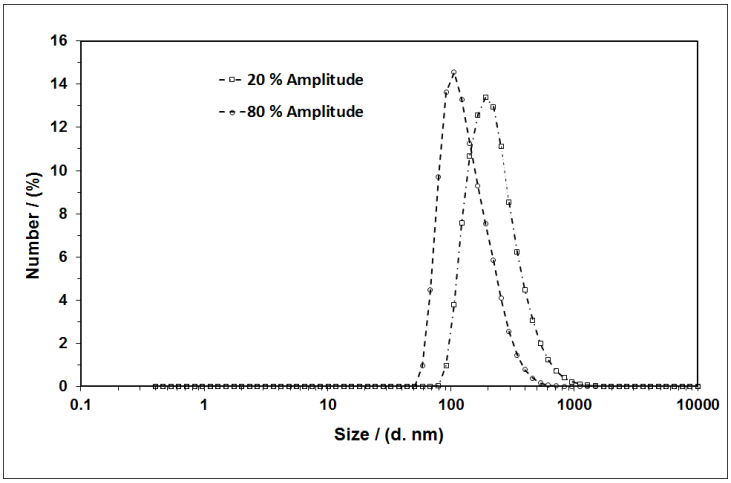
Number / (%)
Size / (d. nm)
20 % Amplitude
80 % Amplitude
0
2
4
6
8
10
12
14
16
0.1
1
10
100
1000
10000

Figure 4.

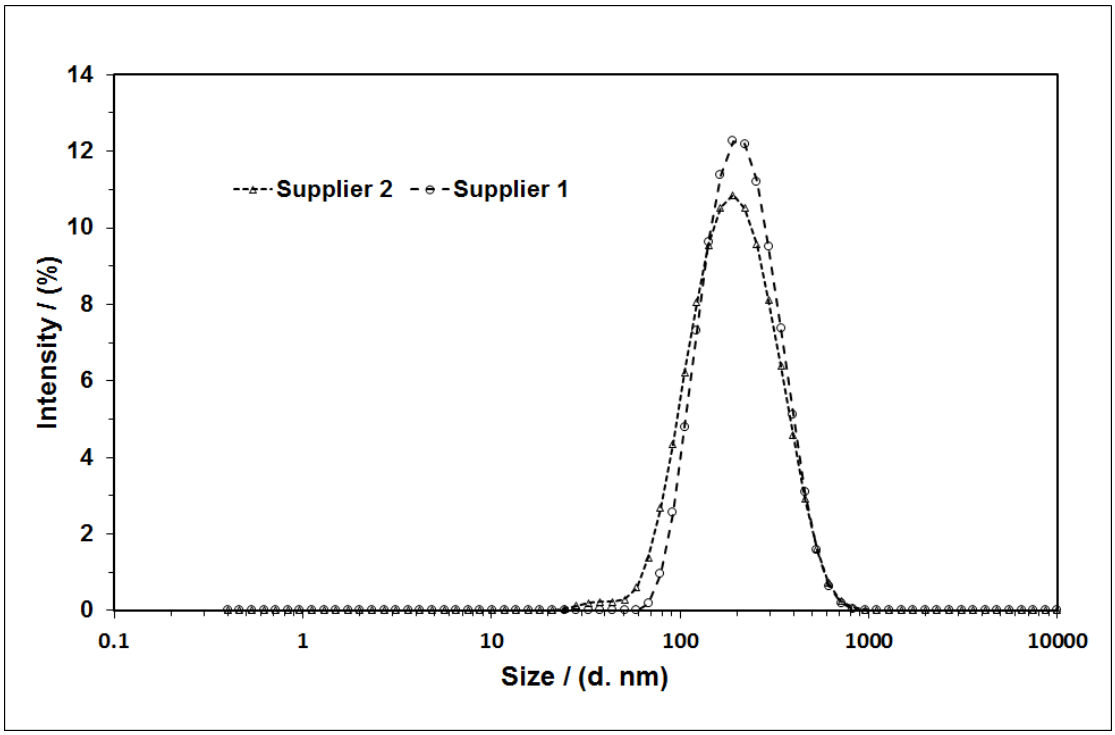
Supplier 2
Supplier 1
Intensity / (%)
Size / (d. nm)
0
2
4
6
8
10
12
14
0.1
1
10
100
1000
10000

Figure 5

(a)

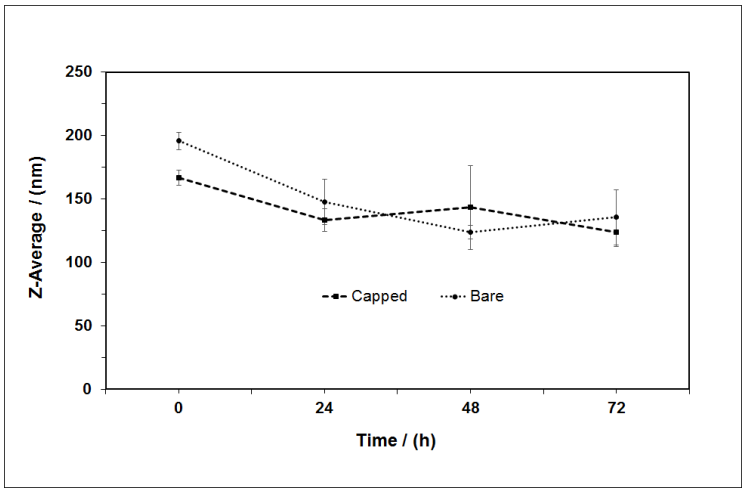
Z-Average / (nm)
250
200
150
100
50
0
Capped
Bare
0
24
48
72
Time / (h)

(b)

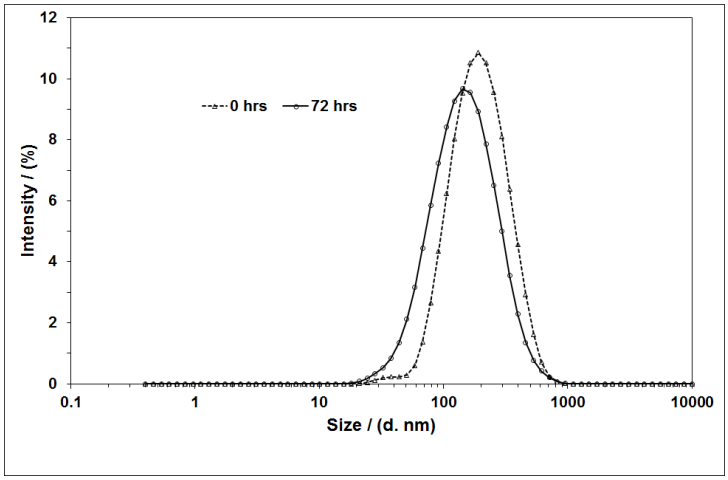
Intensity / (%)
12
10
8
6
4
2
0
0 hrs
72 hrs
0.1
1
10
100
1000
10000
Size / (d. nm)

(c)

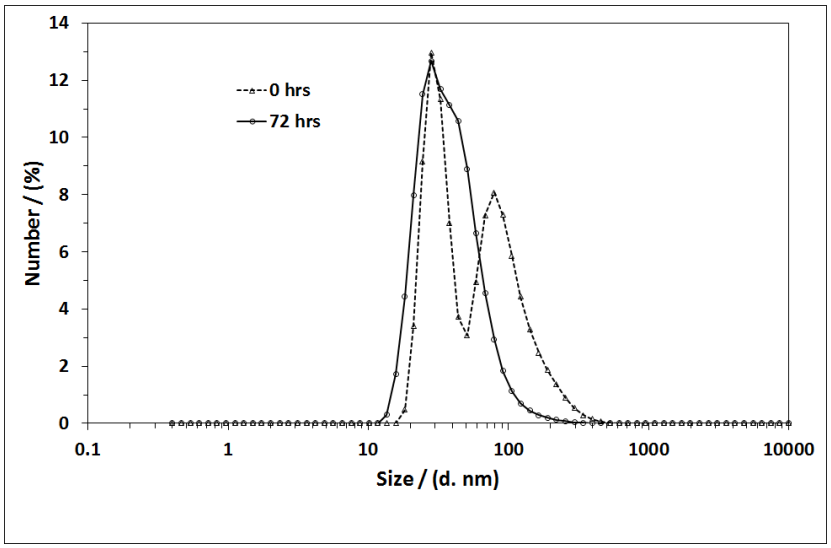
Number / (%)
14
12
10
8
6
4
2
0
0 hrs
72 hrs
0.1
1
10
100
1000
10000
Size / (d. nm)

Figure 6.

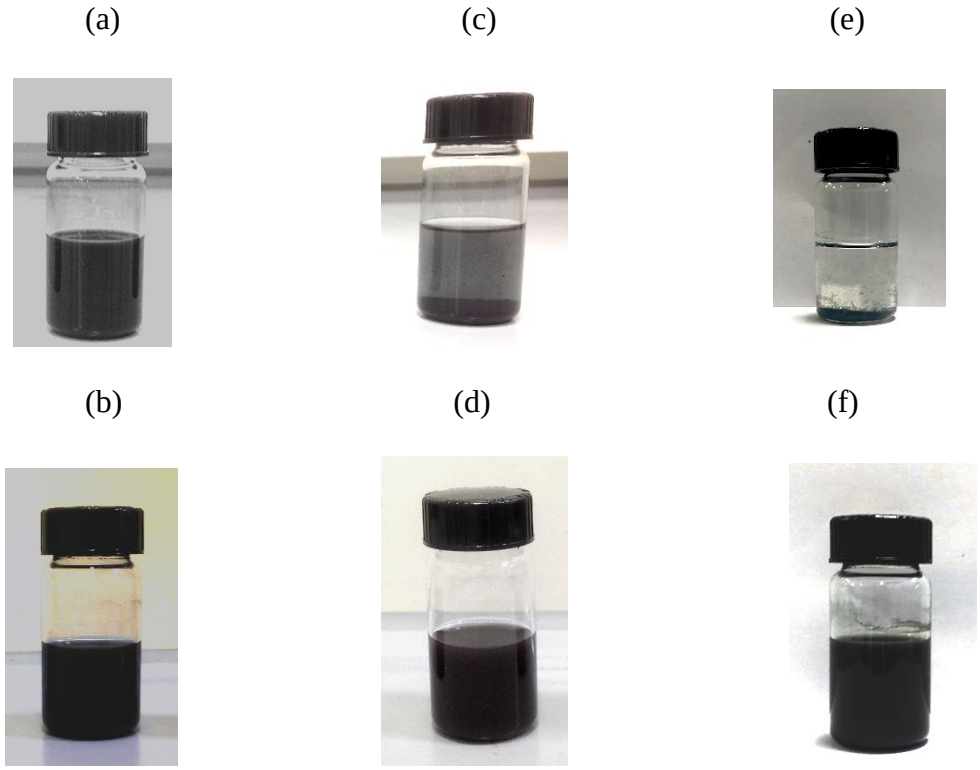

Figure 7.

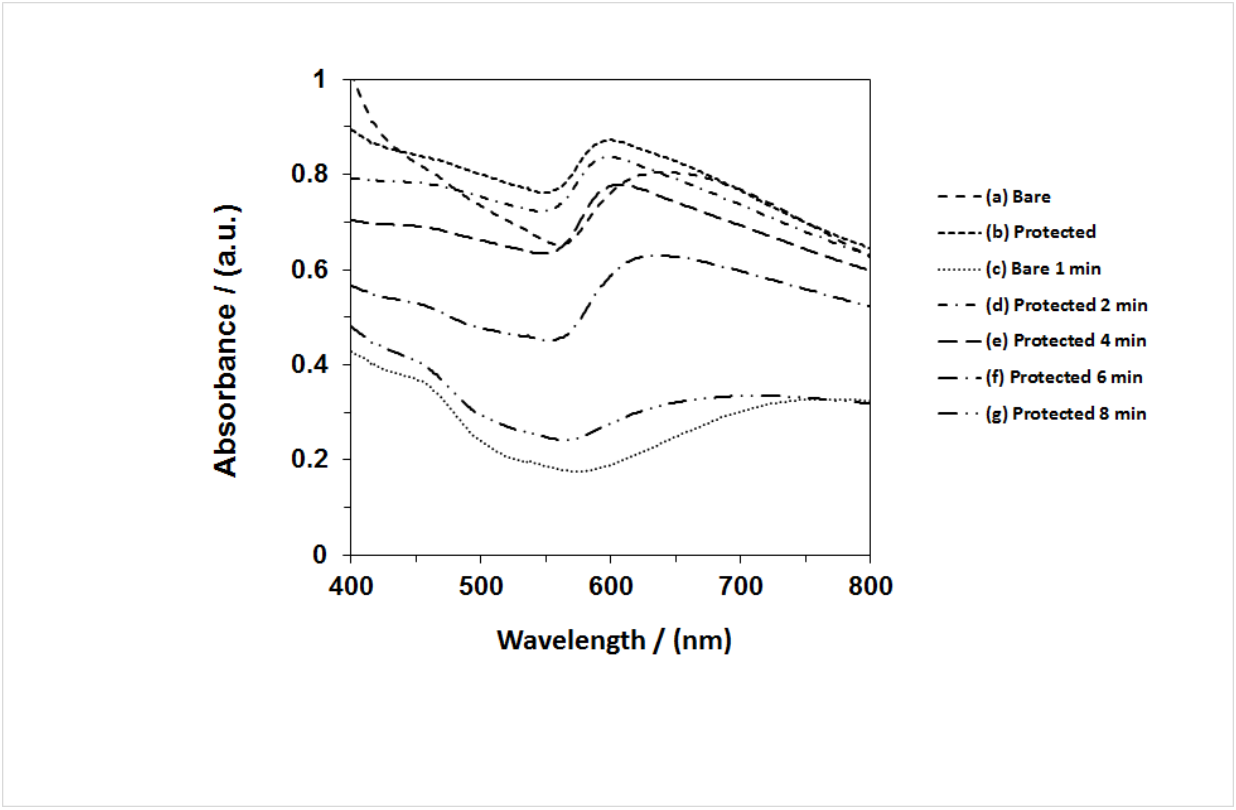
Absorbance / (a.u.)
1
0.8
0.6
0.4
0.2
0
400
500
600
700
800
Wavelength / (nm)
(a) Bare
(b) Protected
(c) Bare 1 min
(d) Protected 2 min
(e) Protected 4 min
(f) Protected 6 min
(g) Protected 8 min

Figure 8.

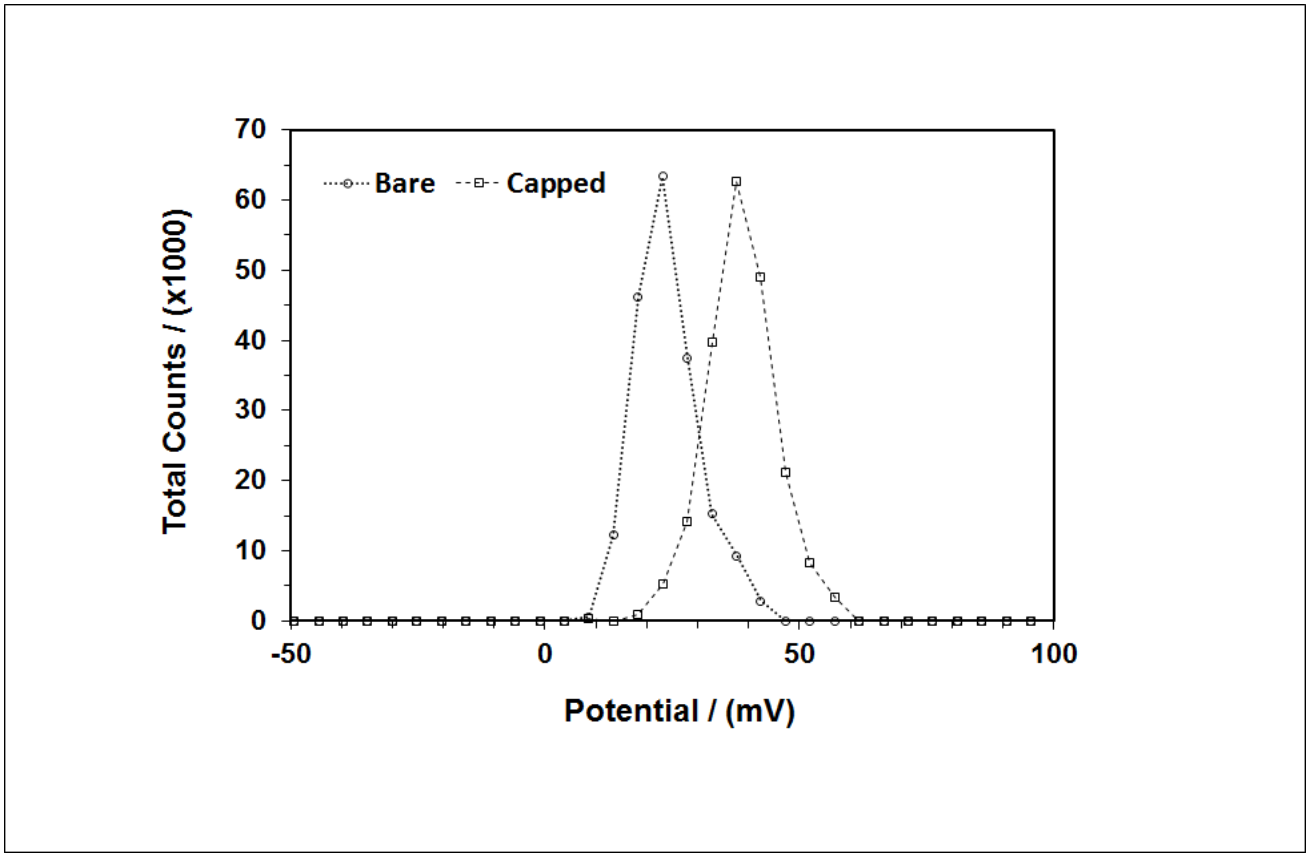
Bare
Capped
Total Counts / (x1000)
70
60
50
40
30
20
10
0
-50
0
50
100
Potential / (mV)

Figure 9.

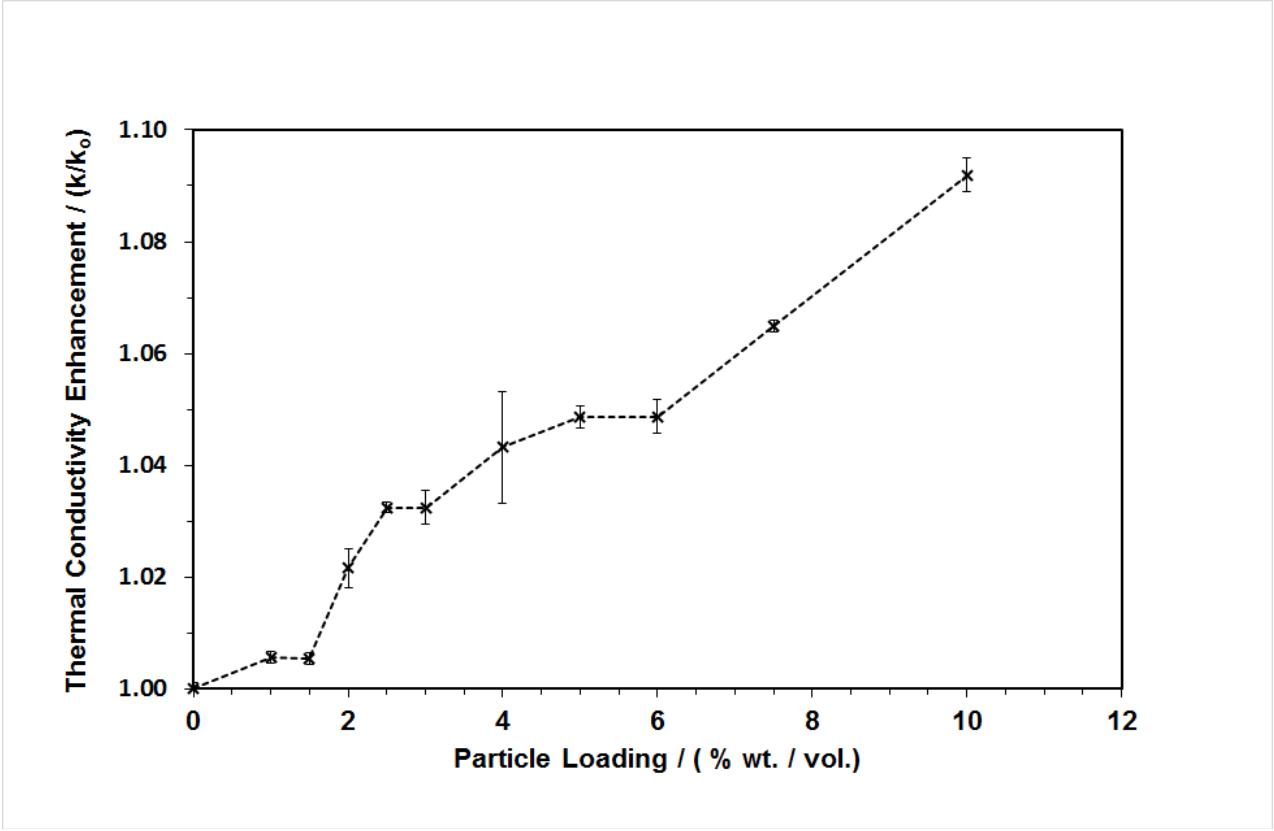
Thermal Conductivity Enhancement / (k/k$_o$)
1.10
1.08
1.06
1.04
1.02
1.00
0
2
4
6
8
10
12
Particle Loading / (% wt. / vol.)